HDL-TM-92-25

September 1992

Energy Levels and Predicted Absorption Spectra of Rare-Earth Ions in Rare-Earth Arsenides

by Donald E. Wortman and Clyde A. Morrison

U.S. Army Laboratory Command
Harry Diamond Laboratories
Adelphi, MD 20783-1197

The findings in this report are not to be construed as an official Department of the Army position unless so designated by other authorized documents.

Citation of manufacturer's or trade names does not constitute an official endorsement or approval of the use thereof.

Destroy this report when it is no longer needed. Do not return it to the originator.

REPORT DOCUMENTATION PAGE

Form Approved
OMB No. 0704-0188

1. AGENCY USE ONLY *(Leave blank)*	2. REPORT DATE	3. REPORT TYPE AND DATES COVERED
	September 1992	Interim, from 1 July to 30 Sept 1992

4. TITLE AND SUBTITLE
Energy Levels and Predicted Absorption Spectra of Rare-Earth Ions in Rare-Earth Arsenides

5. FUNDING NUMBERS

6. AUTHOR(S)
Donald E. Wortman and Clyde A. Morrison

7. PERFORMING ORGANIZATION NAME(S) AND ADDRESS(ES)
Harry Diamond Laboratories
2800 Powder Mill Road
Adelphi, MD 20783-1197

8. PERFORMING ORGANIZATION REPORT NUMBER
HDL-TM-92-25

9. SPONSORING/MONITORING AGENCY NAME(S) AND ADDRESS(ES)
U.S. Army Laboratory Command
2800 Powder Mill Road
Adelphi, MD 20783-1145

10. SPONSORING/MONITORING AGENCY REPORT NUMBER

11. SUPPLEMENTARY NOTES
AMS code: 612120H25
HDL PR: 2R8A51

12a. DISTRIBUTION/AVAILABILITY STATEMENT
Approved for public release; distribution unlimited.

12b. DISTRIBUTION CODE

13. ABSTRACT *(Maximum 200 words)*

A crystal-field Hamiltonian for octahedral symmetry was used along with free-ion parameters for aqueous solution to fit the reported optical absorption spectra of Er^{3+} in ErAs. Parameters obtained from this fit were then used in a model to predict optical absorption spectra of Er^{3+} for the $^4I_{15/2}$ to $^4I_{13/2}$ multiplets at 5, 74, and 300 K; these predictions showed excellent agreement with the reported experimental data at these temperatures. Consequently, we used an interpolation procedure to predict the crystal-field splittings of the lower multiplets of the rare-earth ions Tb^{3+} through Yb^{3+} in their respective arsenide compounds. The lowest multiplet energy levels predicted for Tm^{3+} and Yb^{3+} compare favorably with measurements made by inelastic neutron scattering. In addition, we calculate the absorption spectra for Tb^{3+}, Dy^{3+}, Ho^{3+}, Tm^{3+}, and Yb^{3+} in their respective arsenide compounds at 4.2, 77, and 300 K. From these calculations, we show the transitions between the levels of the lowest two J multiplets for each of the ions.

14. SUBJECT TERMS	15. NUMBER OF PAGES
Rare-earth arsenides, rare-earth spectra	29
	16. PRICE CODE

17. SECURITY CLASSIFICATION OF REPORT	18. SECURITY CLASSIFICATION OF THIS PAGE	17. SECURITY CLASSIFICATION OF ABSTRACT	20. LIMITATION OF ABSTRACT
Unclassified	Unclassified	Unclassified	UL

Contents

1. Introduction 5
2. Fitting Experimental Data 5
3. Calculation of Magnetic Dipole Line Strengths 7
4. Comparison with Experiment 8
5. Emission Branching Ratios 8
6. Theoretical Predictions 10
7. Predicted Energy Levels, *g* Values, Absorption Spectra, and Multiplet Branching Ratios 12
7.1 Tb in TbAs 12
7.2 Dy in DyAs 14
7.3 Ho in HoAs 16
7.4 Tm in TmAs 18
7.5 Yb in YbAs 20
8. Conclusion 22
Acknowledgements 22
References 23
Distribution 25

Figures

1. Predicted absorption spectra of $^4I_{15/2}$ to $^4I_{13/2}$ levels of Er^{3+} in ErAs, assuming a Lorentzian line shape with $\Delta E = 3$ cm^{-1} 9
2. Four largest line-to-line branching ratios at 300 K for $^4I_{13/2}$ to $^4I_{15/2}$ transitions for Er^{3+} in ErAs 10
3. Predicted absorption spectra of $^7F_6$ to $^7F_5$ levels of Tb^{3+} in TbAs, assuming a Lorentzian line shape with $\Delta E = 3$ cm^{-1} 13
4. Multiplet-to-multiplet branching ratios for Dy^{3+} in DyAs 15
5. Predicted absorption spectra of $^6H_{15/2}$ to $^6H_{13/2}$ levels of Dy^{3+} in DyAs, assuming a Lorentzian line shape with $\Delta E = 3$ cm^{-1} 15
6. Predicted absorption spectra of $^5I_8$ to $^5I_7$ levels of Ho^{3+} in HoAs, assuming a Lorentzian line shape with $\Delta E = 3$ cm^{-1} 17
7. Predicted absorption spectra of $^3H_6$ to $^3F_4$ levels of Tm^{3+} in TmAs, assuming a Lorentzian line shape with $\Delta E = 3$ cm^{-1} 19
8. Predicted absorption spectra of $^2F_{7/2}$ to $^2F_{5/2}$ levels of Yb^{3+} in YbAs, assuming a Lorentzian line shape with $\Delta E = 3$ cm^{-1} 21

Tables

1. Theoretical and experimental energy levels 6
2. Magnetic dipole line strengths, S_{nm}, for line-to-line $^4I_{15/2} \leftrightarrow {}^4I_{13/2}$ 7
3. g values of $^4I_{15/2}$ and $^4I_{13/2}$ levels of Er^{3+} in ErAs 7
4. Lattice constants for *Ln*As for experimental values and interpolated values for triply ionized rare-earth ions with electronic configuration $4f^N$ 11
5. Interpolated crystal-field components, A_{kq}, and crystal-field parameters, B_{nm}, for *Ln*As 11
6. Predicted energy levels and free-ion mixture for Tb^{3+} in TbAs 12
7. Predicted g values for Γ_4 and Γ_5 levels of Tb^{3+} in TbAs 13
8. Predicted energy levels and free-ion mixture for Dy^{3+} in DyAs 14
9. Predicted g values for Γ_6, Γ_7, and Γ_8 levels of Dy^{3+} in DyAs 16
10. Predicted energy levels and free-ion mixture for Ho^{3+} in HoAs 16
11. Predicted g values for Γ_4 and Γ_5 levels of Ho^{3+} in HoAs 17
12. Predicted energy levels and free-ion mixture for Tm^{3+} in TmAs 18
13. Predicted g values for Γ_4 and Γ_5 levels of Tm^{3+} in TmAs 19
14. Experimental energy levels of Tm^{3+} in TmAs reported by Hulliger [10] 19
15. Comparison of present work and Hulliger [10] 19
16. Predicted energy levels and free-ion mixture for Yb^{3+} in YbAs 20
17. Predicted g values for Γ_6, Γ_7, and Γ_8 of Yb^{3+} in YbAs 21

1. Introduction

Small, stable, narrow-linewidth lasers built by the doping of rare-earth ions in III-V semiconductors are of current interest for optoelectronic components and integrated optical circuits. Lasers with these desirable properties can be pumped by photons whose energies are greater than the band gap or by current injection into the region occupied by the rare-earth ions. Characteristic, narrow-line frequencies of the $4f^N$ rare-earth ions can provide direct laser output or can be used to lock III-V semiconductor laser transitions [1].

In the work reported here, we analyze the absorption spectra [2] of Er^{3+} in a 3300-Å-thick layer of ErAs to obtain phenomenological crystal-field parameters, B_{nm}, for Er^{3+} in ErAs. The B_{nm} were obtained by least-squares fitting the reported spectra on the $^4I_{15/2}$ and $^4I_{13/2}$ multiplets of Er^{3+}, and these were also used to calculate the magnetic dipole line strengths for all the transitions, as well as the magnetic g factors for each level. The magnetic dipole line strengths were then used to compute the absorption spectra of Er^{3+} in ErAs; the computation results compare favorably with experiment. The line-to-line emission branching ratios were calculated as a function of temperature for the $^4I_{13/2}$ to $^4I_{15/2}$ transitions of Er^{3+} in ErAs. Using these B_{nm} for Er, we next predict the B_{nm} for the entire triply ionized rare-earth series of arsenides, LnAs (Ln = Ce to Yb). These latter B_{nm} are then used to predict the energy levels and the magnetic dipole line strengths for triply ionized Tb, Dy, Ho, Er, Tm, and Yb in their respective arsenide lattices. We present the absorption spectra calculated for transitions between the levels of the lowest two J multiplets of these ions, assuming a Lorentzian lineshape with a linewidth of 3 cm^{-1}. Much of the analysis follows the procedure used previously [3] in the investigation of the spectra of triply ionized lanthanides (rare-earth ions), Ln^{3+}, in $Cs_2NaLnCl_6$.

The phenomenological A_{nm} for Er^{3+} in ErAs were obtained from the relation $B_{nm} = \rho_n A_{nm}$, where the ρ_n for each rare-earth ion were given in 1979 by Morrison and Leavitt [4]. These phenomenological A_{nm} for ErAs and the 1968 x-ray data of Wyckoff [5] yielded B_{nm}, which were used to compute the energy levels and multiplet branching ratios for the triply ionized rare-earth ions, LnAs, for Tb^{3+} through Yb^{3+}. The free-ion aqueous parameters of Carnall et al [6] were used in all these calculations.

2. Fitting Experimental Data

In 1991, Schneider et al [2] reported the absorption spectra of Er^{3+} in ErAs at 5, 74, and 300 K and gave an analysis of the energy levels using the Hamiltonian of Lea et al [7] in 1962. The ErAs they investigated was a 3300-Å-thick layer grown by molecular beam epitaxy on a substrate of GaAs capped by a thin layer of GaAs.

The data of Schneider et al [2] were used along with the crystal-field Hamiltonian, H_{CEF}, for the $4f^N$ electronic configuration in O_h symmetry, given by

$$H_{CEF} = B_{40}\sum_{i=1}^{N}\left\{C_{40}(\hat{r}_i) + \sqrt{\frac{5}{14}}\left[C_{44}(\hat{r}_i) + C_{4-4}(\hat{r}_i)\right]\right\} + B_{60}\sum_{i=1}^{N}\left\{C_{60}(\hat{r}_i) - \sqrt{\frac{7}{2}}\left[C_{64}(\hat{r}_i) + C_{6-4}(\hat{r}_i)\right]\right\}, \quad (1)$$

to obtain the best least-squares fit between the calculated and measured energy levels. In obtaining the best fit to the experimental data, we varied B_{40} and B_{60} as well as the calculated difference in the centroids of the $^4I_{15/2}$ and $^4I_{13/2}$ multiplets. The free-ion wavefunctions were determined from the parameters [6] for aqueous solution. Because we could not convert the parameters B_4 and B_6 of Schneider et al [2] to the form used in equation (1), we started the fit with the B_{40} and B_{60} values given elsewhere [3] for Er^{3+} in $Cs_2NaErCl_6$. The reason for this choice is that the point-group symmetry for Er^{3+} in ErAs and in $Cs_2NaErCl_6$ is the same in each material (O_h). Again, as before [3], we label the states according to their transformation properties under the group O rather than O_h. This entails dropping the parity labels (+) or (–), which are determined by the number of f electrons. The irreducible representations of the O group are from Koster et al [8]. The resulting parameters, energy levels, and wavefunction compositions are given in table 1.

Table 1. Theoretical and experimental energy levels (cm^{-1}) and composition for Er^{3+} in ErAs[a]

No.[b]	Centroid[c]	I. R.[d]	$E_{Theo.}$	$E_{Exp.}$[e]		Free-ion mixture (%)
1	61	Γ_8	0.3	0	99.99	$^4I_{15/2}$
2		Γ_7	26.4	27.2	99.99	$^4I_{15/2} + 0.01\ ^4I_{13/2}$
3		Γ_8	28.6	27.2	99.99	$^4I_{15/2} + 0.01\ ^4I_{13/2}$
4		Γ_6	126.8	129.0	100.00	$^4I_{15/2}$
5		Γ_8	133.5	133.5	99.99	$^4I_{15/2}$
6	6534	Γ_6	6490.7	6491.3	99.99	$^4I_{13/2}$
7		Γ_8	6505.4	6505.7	99.97	$^4I_{13/2} + 0.03\ ^4I_{11/2}$
8		Γ_7	6515.4	6515.7	99.96	$^4I_{13/2} + 0.03\ ^4I_{11/2}$
9		Γ_7	6582.6	6583.0	99.99	$^4I_{13/2} + 0.01\ ^4I_{15/2}$
10		Γ_8	6583.9	6583.0	99.99	$^4I_{13/2} + 0.01\ ^4I_{15/2}$
11	10,220	Γ_6	10194.8	—	99.97	$^4I_{11/2} + 0.01\ ^4I_{9/2} + 0.01\ ^4F_{7/2}$
12		Γ_8	10201.2	—	99.95	$^4I_{11/2} + 0.04\ ^4I_{9/2}$
13		Γ_7	10236.5	—	99.96	$^4I_{11/2} + 0.03\ ^4I_{13/2}$
14		Γ_8	10239.9	—	99.97	$^4I_{11/2} + 0.02\ ^4I_{13/2}$

[a] B_{40} = 704.5, B_{60} = 51.07 cm^{-1}, and rms = 0.870 cm^{-1}.
[b] Numbers used to designate levels used in discussion.
[c] In absence of experimental data, centroids were calculated from aqueous solution parameters of Carnall et al [6].
[d] Irreducible representation of O group, Koster et al [8].
[e] Tsang and Logan [1].

3. Calculation of Magnetic Dipole Line Strengths

Since the Er^{3+} ion occupies a site with O_h symmetry, the electric dipole transitions are parity forbidden. However, the magnetic dipole operator has even parity and should correspond to the experimental absorption, if we assume that the absorption is not vibrationally assisted. Because of the excellent agreement of the calculated values of the energy levels with the experimental values, we assume that all the observed levels are magnetic dipole. The operator we use for the magnetic dipole, **M**, is

$$\mathbf{M} = \frac{\alpha a_o}{2}(\mathbf{L} + g_e\mathbf{S}) \ , \tag{2}$$

where α is the fine structure constant, a_o the Bohr radius, g_e the free-electron g-factor, and **L** and **S** are the orbital and spin operators, respectively. We then calculate the line strength given by

$$S_{nm} = \sum_{i,f} |\langle m\Gamma_f|\mathbf{M}|n\Gamma_i\rangle|^2 \ , \tag{3}$$

where the sum on i and f is over all the components of Γ_i and Γ_f. The wavefunctions $|n\Gamma_i\rangle$ and $|m\Gamma_f\rangle$ are obtained from the simultaneous diagonalization of the crystal field in equation (1) and the free-ion Hamiltonian with the parameters for Er^{3+} given by Carnall et al [6]. These results are given in table 2. We also calculated the g values as defined earlier [3] for the $^4I_{15/2}$ and $^4I_{13/2}$ energy levels; these results are given in table 3.

Table 2. Magnetic dipole line strengths, S_{nm} (10^{-23} cm^2), for line-to-line $^4I_{15/2} \leftrightarrow {}^4I_{13/2}$

n, Γ_j \ m, Γ_i	6, Γ_6	7, Γ_8	8, Γ_7	9, Γ_7	10, Γ_8
1, Γ_8	47.73	30.74	3.139	0.01178	0.3887
2, Γ_7	0	6.804	8.717	1.060	3.290
3, Γ_8	0.0015	33.16	14.69	8.120	8.001
4, Γ_6	0.0028	0.0032	0	0	44.75
5, Γ_8	0.0398	0.2482	0.2345	38.43	40.15

Table 3. g values of $^4I_{15/2}$ and $^4I_{13/2}$ levels of Er^{3+} in ErAs[a]

No.	I. R.	g_1	g_2
1	Γ_8	4.945	−11.897
2	Γ_7	—	6.777
3	Γ_8	−1.194	9.697
4	Γ_6	−5.933	—
5	Γ_8	−12.174	0.215
6	Γ_6	5.546	—
7	Γ_8	−2.506	−5.996
8	Γ_7	—	−3.642
9	Γ_7	—	4.285
10	Γ_8	0.294	9.737

[a] *For an explanation of definition of notation of g values, see Morrison et al [3].*

4. Comparison with Experiment

The line strengths given in table 2 have been used to calculate the line-to-line absorption as a function of energy at 5, 74, and 300 K reported by Schneider et al [2]. The results are shown in figure 1. The quantity plotted, $I(E)$, is

$$I(E) = \sum_{j=6}^{10} \sum_{i=1}^{5} \frac{(E_j - E_i) S_{ij} \exp\left[-(E_i - E_1)/kT\right]}{\left\{\left[E - (E_j - E_i)\right]^2 + (\Delta/2)^2\right\} Z_1}, \tag{4}$$

where

$$Z_1 = \sum_{i=1}^{5} w_i \exp\left[-(E_i - E_1)/kT\right] \tag{5}$$

and Δ is the full linewidth at half maximum value, and, as suggested by Schneider et al [2], we have used $\Delta = 3\ \mathrm{cm}^{-1}$. If this figure is compared with figure 1 of Schneider et al [2], we find that every line agrees with their results, except for the splittings of the lines they label 1 and 2.

5. Emission Branching Ratios

We calculated the emission branching ratios assuming that the $^4I_{13/2}$ level is pumped and the population of this state is thermalized. That is, we calculate

$$\beta_{ij} = \frac{\exp[-(E_j - E_6)/kT] S_{ij} (E_j - E_i)^3}{S_o Z_2} \tag{6}$$

for $j = 6$ to 10, $i = 1$ to 5, where

$$Z_2 = \sum_{j=6}^{10} w_j \exp[-(E_j - E_6)/kT]; \tag{7}$$

S_o is determined such that

$$1 = \sum_{i=1}^{5} \sum_{j=6}^{10} \beta_{ij},$$

and w_j is the degeneracy of each level in the $^4I_{13/2}$ multiplet ($w_j = 2$ for Γ_6 and Γ_7, and 4 for Γ_8). The β_{ij} are shown in figure 2 for the four largest branching ratios at $T = 300$ K. At all temperatures, the largest branching ratio is from level 6 to level 1 ($\Delta E = 6491.3\ \mathrm{cm}^{-1}$). However, at room temperatures, the transition of level 7 to level 3 ($\Delta E = 6478.5\ \mathrm{cm}^{-1}$) has a large branching ratio

(13.4 percent), but since level 3 is only 27.2 cm^{-1} above the ground level, population inversion would be difficult. Also, at room temperature, it might be possible to achieve population inversion in the transition from level 10 to level 4 (β = 12.5 percent) at 129 cm^{-1} (ΔE = 6454.0 cm^{-1}).

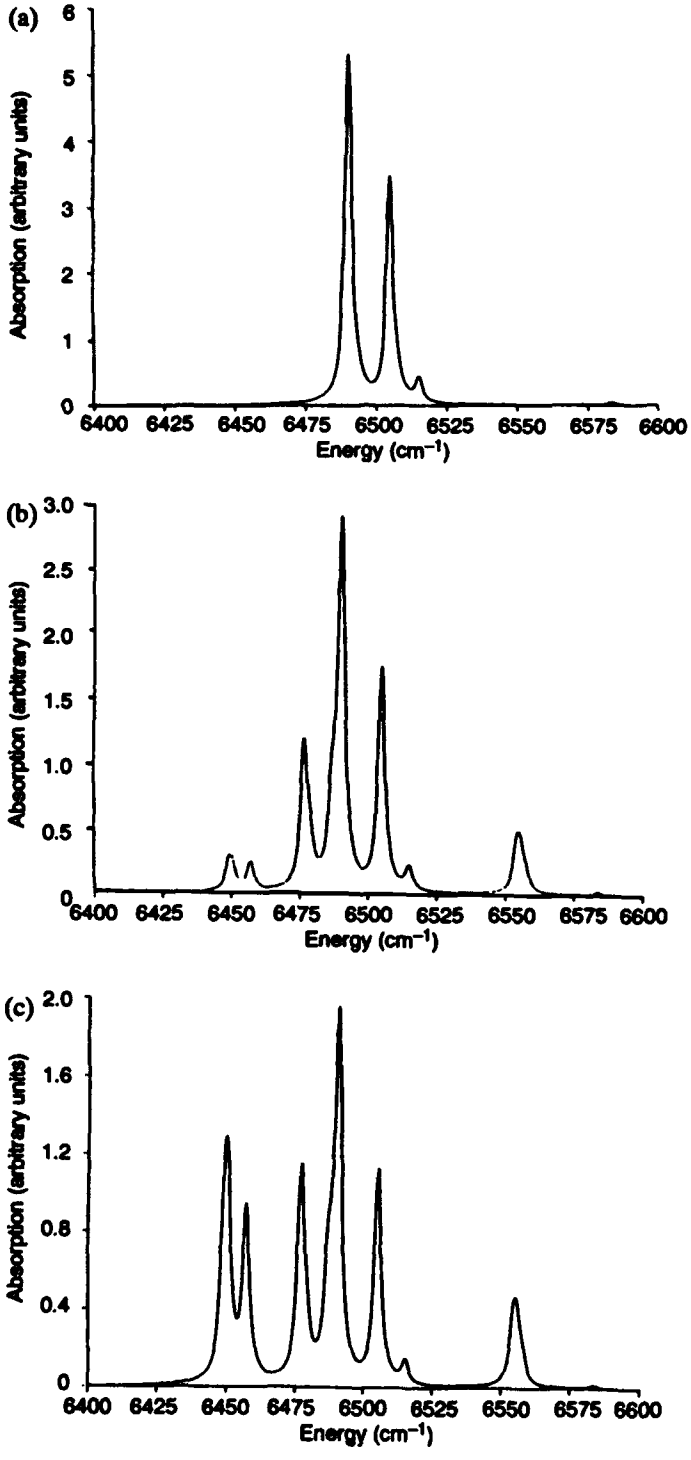

Figure 1. Predicted absorption spectra of $^4I_{15/2}$ to $^4I_{13/2}$ levels of Er^{3+} in ErAs, assuming a Lorentzian line shape with ΔE = 3 cm^{-1}:
(a) T = 5 K,
(b) T = 74 K, and
(c) T = 300 K.

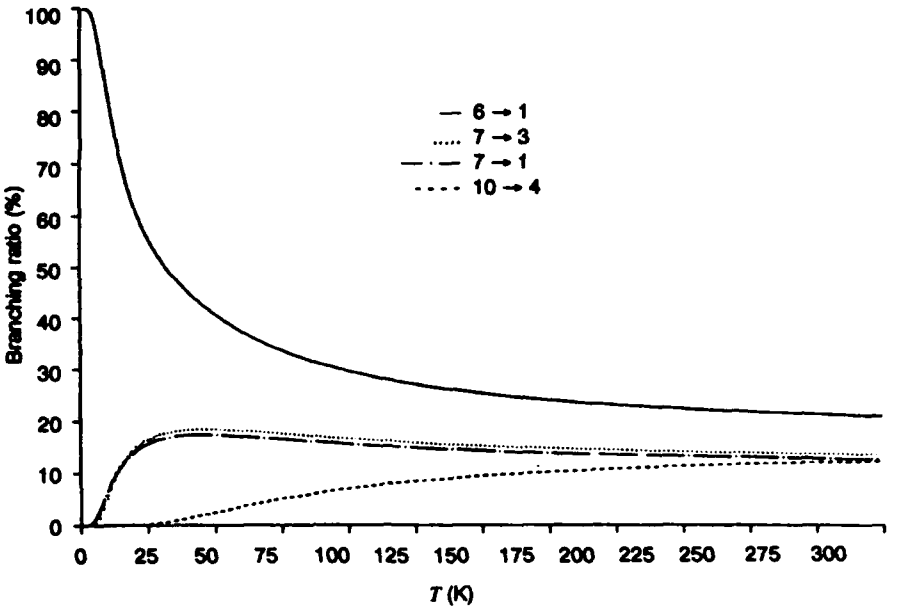

Figure 2. Four largest line-to-line branching ratios at 300 K for $^4I_{13/2}$ to $^4I_{15/2}$ transitions for Er^{3+} in ErAs.

6. Theoretical Predictions

In the three-parameter theory of crystal fields proposed in 1975 by Leavitt et al [9], the crystal-field parameters, B_{nm}, are related to the crystal-field components by

$$B_{nm} = \rho_n A_{nm} , \tag{8}$$

and it is assumed that the ρ_n are dependent only on the lanthanide ion and the A_{nm} are host dependent. In the cubic symmetry for the *Ln*As compounds, we need only ρ_4 and ρ_6 along with A_{40} and A_{60}. The values for ρ_n have been tabulated elsewhere [4], and we use these values here. Using the values of ρ_4 and ρ_6 for Er^{3+} and the values of B_{40} and B_{60} from the best fit given in table 1, we obtain experimental values of the crystal components A_{40}(Er) and A_{60}(Er), which can be used in equation (8) to predict the energy levels of the other lanthanides as impurities in ErAs. However, we wish to find the $A_{nm}(Ln)$ in *Ln*As. To obtain the $A_{nm}(Ln)$ for *Ln*As, we assume that the dominant contribution to the $A_{nm}(Ln)$ is given by the monopole contribution to the crystal-field components. For cubic site symmetry, the monopole A_{nm} can be written as

$$A_{nm}(Ln) = V_{nm}/a(Ln)^{n+1} , \tag{9}$$

where $a(Ln)$ is the lattice constant for *Ln*As and the V_{nm} are crystal-field components for the unit lattice constant and are the same for all cubic *Ln*As. The $a(Ln)$ for a number of lanthanides are given by Wyckoff [5], and his results have been used to interpolate the lattice constants for all the *Ln*As from LaAs through LuAs; these results are given in table 4.

We obtain the $A_{nm}(Ln)$ for LnAs from equation (9) by using

$$A_{nm}(Ln) = A_{nm}(\mathrm{Er})\left[\frac{a\,(\mathrm{Er})}{a\,(Ln)}\right]^{n+1} \tag{10}$$

with the A_{nm}(Er) determined from the phenomenological B_{40} and B_{60} for Er in ErAs. These results are given in table 5, along with the B_{40} and B_{60} for all the LnAs given in table 4. If the values of B_{40} and B_{60} in table 5 are compared to the values given earlier [3] (table VI) for Ln^{3+} in $Cs_2NaLnCl_6$, we see that the B_{40} and B_{60} are much smaller for LnAs.

Table 4. Lattice constants for LnAs (Ln = La to Lu) for experimental values and interpolated values for triply ionized rare-earth ions with electronic configuration $4f^N$

N	Ion	a (Å)[a]	a (Å)[b]
0	La	6.125	6.103
1	Ce	6.060	6.060
2	Pr	5.997	6.019
3	Nd	5.958	5.980
4	Pm	—	5.943
5	Sm	5.921	5.908
6	Eu	—	5.875
7	Gd	5.854	5.844
8	Tb	5.827	5.814
9	Dy	5.780	5.787
10	Ho	5.771	5.762
11	Er	5.732	5.738
12	Tm	5.711	5.717
13	Yb	5.698	5.697
14	Lu	—	5.679

[a] *R.W.G. Wyckoff [5].*
[b] $a(N) = 6.103273 - 4.378697X + 9.666212X^2$, $X = N/100$ (rms = 1.326×10^{-2} Å)

Table 5. Interpolated crystal-field components, A_{kq}, and crystal-field parameters, B_{nm}, for LnAs

N	Ion	A_{40} (cm^{-1}/Å^4)	B_{40} (cm^{-1})	A_{60} (cm^{-1}/Å^6)	B_{60} (cm^{-1})
0	La	1254	—	33.76	—
1	Ce	1299	979.4	35.47	83.06
2	Pr	1344	869.0	37.19	69.75
3	Nd	1388	802.1	38.92	61.87
4	Pm	1432	764.8	40.65	57.79
5	Sm	1475	745.0	42.37	55.97
6	Eu	1517	733.9	44.07	55.10
7	Gd	1558	725.7	45.74	54.31
8	Tb	1598	717.6	47.38	53.22
9	Dy	1636	710.4	48.97	51.98
10	Ho	1672	705.4	50.50	51.11
11	Er	1707	704.5	51.97	51.07
12	Tm	1739	705.1	53.36	51.48
13	Yb	1770	697.0	54.66	49.85
14	Lu	1797	—	55.86	—

7. Predicted Energy Levels, g Values, Absorption Spectra, and Multiplet Branching Ratios

The B_{40} and B_{60} in table 5 are used in equation (1) along with the free-ion centroids of Carnall et al [6] from the aqueous data to obtain the energy levels, g values, absorption spectra, and branching ratios for Ln = Tb, Dy, Ho, Tm, and Yb in LnAs. Only the multiplets that lie in the band gap of GaAs (~11,000 cm^{-1}) are given.

7.1 Tb in TbAs

The energy levels and free ion composition of the wavefunctions for the ^7F_J for J = 6 through 0 are given in table 6. For most values of J, the free-ion component of the wavefunction exceeds 99 percent, and this result would indicate that the analysis of the experimental data using the operator equivalent method given by Lea et al [7] would give a good representation of the crystal-field parameters. The strongest optical absorption would be in the 2000 cm^{-1} region ($^7F_6 \rightarrow {}^7F_5$), which is the long wavelength limit given by Schneider et al [2]. Multiplet line strengths of $^7F_6$ to higher multiplets are two

Table 6. Predicted energy levels and free-ion mixture for Tb^{3+} in TbAs[a]

No.[b]	Centroid[c]	I. R.[d]	Energy (cm^{-1})	Free-ion mixture (%)
1	74	Γ_1	0.0	99.86 $^7F_6$ + 0.13 $^7F_4$
2		Γ_4	17.8	99.75 $^7F_6$ + 0.16 $^7F_5$ + 0.08 $^7F_4$
3		Γ_5	38.6	99.62 $^7F_6$ + 0.35 $^7F_5$ + 0.02 $^7F_4$
4		Γ_2	121.5	99.94 $^7F_6$ + 0.06 $^7F_3$
5		Γ_5	148.6	99.86 $^7F_6$ + 0.09 $^7F_5$ + 0.03 $^7F_4$
6		Γ_3	157.6	99.88 $^7F_6$ + 0.06 $^7F_5$ + 0.05 $^7F_4$
7	2112	Γ_4	2058.3	99.84 $^7F_5$ + 0.11 $^7F_6$ + 0.04 $^7F_1$
8		Γ_5	2112.1	99.43 $^7F_5$ + 0.44 $^7F_6$ + 0.10 $^7F_2$
9		Γ_3	2160.5	99.81 $^7F_5$ + 0.09 $^7F_2$ + 0.06 $^7F_6$
10		Γ_4	2177.3	99.72 $^7F_5$ + 0.19 $^7F_3$ + 0.05 $^7F_6$
11	3370	Γ_1	3309.9	99.56 $^7F_4$ + 0.30 $^7F_0$ + 0.13 $^7F_6$
12		Γ_4	3334.7	99.59 $^7F_4$ + 0.16 $^7F_1$ + 0.13 $^7F_3$
13		Γ_3	3354.9	99.89 $^7F_4$ + 0.05 $^7F_6$ + 0.05 $^7F_5$
14		Γ_5	3466.0	99.38 $^7F_4$ + 0.56 $^7F_3$ + 0.05 $^7F_6$
15	4344	Γ_4	4334.8	99.30 $^7F_3$ + 0.36 $^7F_1$ + 0.20 $^7F_5$
16		Γ_5	4360.5	97.33 $^7F_3$ + 2.03 $^7F_2$ + 0.57 $^7F_4$
17		Γ_2	4395.4	99.94 $^7F_3$ + 0.06 $^7F_6$
18	5028	Γ_5	5012.1	97.86 $^7F_2$ + 2.05 $^7F_3$ + 0.08 $^7F_5$
19		Γ_3	5111.1	99.89 $^7F_2$ + 0.09 $^7F_5$ + 0.01 $^7F_4$
20	5481	Γ_4	5502.8	99.43 $^7F_1$ + 0.38 $^7F_3$ + 0.15 $^7F_4$
21	5703	Γ_1	5722.6	99.70 $^7F_0$ + 0.30 $^7F_4$

[a] B_{40} = 717.6 and B_{60} = 53.22 cm^{-1}.
[b] Numbers to designate levels used in discussion.
[c] Aqueous centroids.
[d] Irreducible representation of O group, Koster et al [8].

orders of magnitude smaller than the $^7F_6 \rightarrow {}^7F_5$ transitions. The absorption spectra for the transitions between the energy levels of the $^7F_6$ to the $^7F_5$ were computed using equation (4) with $1 \leq i \leq 6, 7 \leq j \leq 10$ (table 6) and are shown in figure 3 for $T = 4.2$, 77, and 300 K. In addition, the g values for all the states are given in table 7.

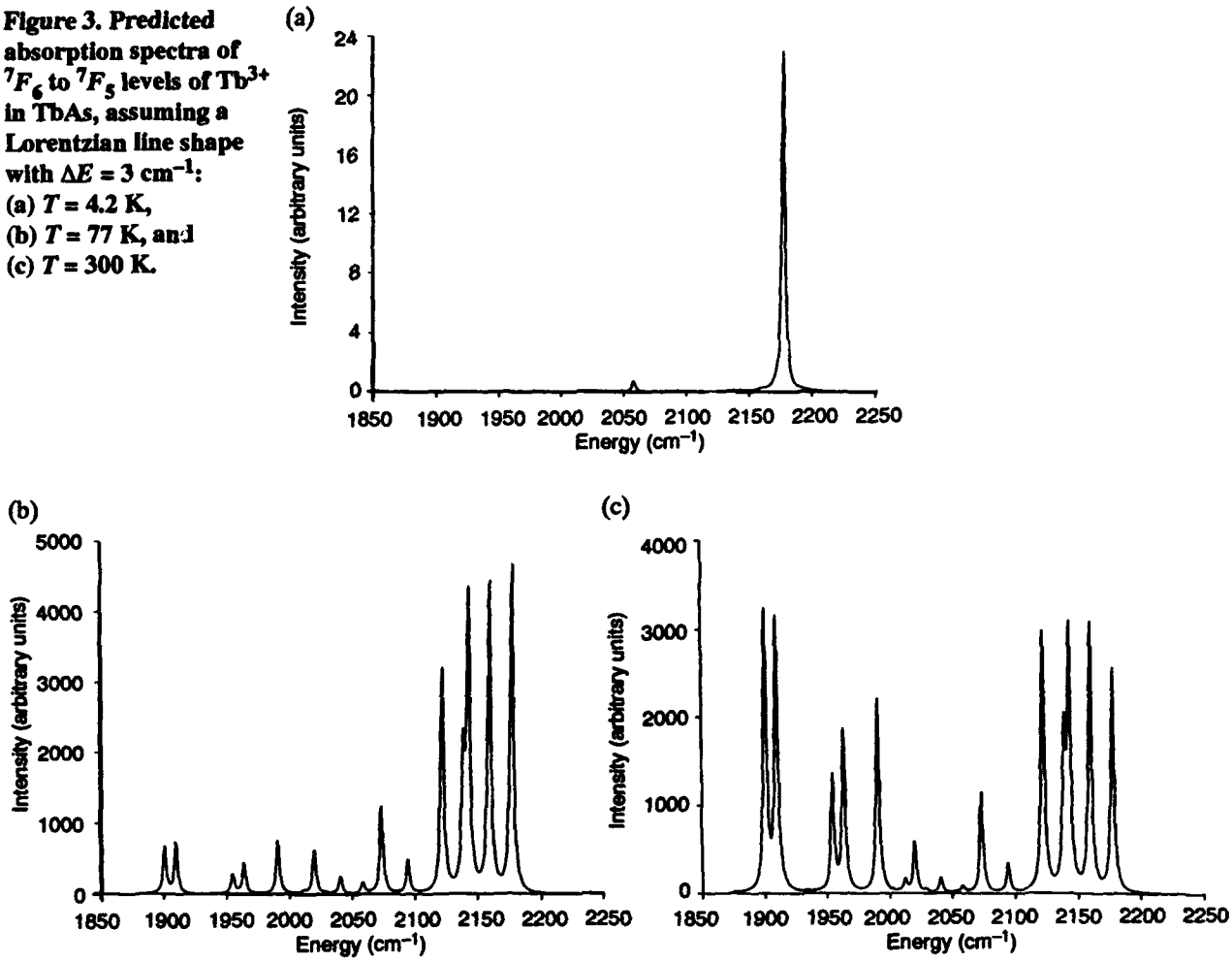

Figure 3. Predicted absorption spectra of $^7F_6$ to $^7F_5$ levels of Tb^{3+} in TbAs, assuming a Lorentzian line shape with $\Delta E = 3$ cm^{-1}:
(a) $T = 4.2$ K,
(b) $T = 77$ K, and
(c) $T = 300$ K.

Table 7. Predicted g values for Γ_4 and Γ_5 levels of Tb^{3+} in TbAs[a]

No.	I. R.	g
2	Γ_4	1.5568
3	Γ_5	5.6857
5	Γ_5	1.7981
7	Γ_4	8.9031
8	Γ_5	7.4531
10	Γ_4	–7.4577
12	Γ_4	1.6281
14	Γ_5	–7.1609
15	Γ_4	–4.6128
16	Γ_5	–1.0517
18	Γ_5	2.2372
20	Γ_4	2.9733

[a]See Morrison et al [3] for definition of g values.

7.2 Dy in DyAs

The energy levels and free-ion wavefunction composition for ^6H_J, $J = 15/2$ through 5/2, and $^6F_{11/2}$, $^6F_{9/2}$, and $^6F_{7/2}$ are given in table 8. Even though the crystal-field parameters are small, the free-ion levels are mixed by the crystal field. In some cases the mixture of different states consists of 40 percent of a state. For example, one level of the labeled $^6F_{9/2}$ multiplet and one level in the multiplet labeled $^6H_{7/2}$ are only 60 percent of their respective multiplets. The multiplet-to-multiplet branching ratios for each multiplet are shown in figure 4. The absorption spectra for the transitions between the energy levels

Table 8. Predicted energy levels and free-ion mixture for Dy^{3+} in DyAs[a]

No.[b]	Centroid[c]	I. R.[d]	Energy (cm^{-1})	Free-ion mixture (%)
1	40	Γ_6	0.0	99.99 $^6H_{15/2}$ + 0.01 $^6F_{11/2}$
2		Γ_8	12.8	99.98 $^6H_{15/2}$ + 0.02 $^6H_{13/2}$
3		Γ_7	85.5	99.90 $^6H_{15/2}$ + 0.09 $^6H_{13/2}$
4		Γ_8	139.2	99.95 $^6H_{15/2}$ + 0.03 $^6H_{13/2}$ + 0.01 $^6F_{9/2}$
5		Γ_8	174.0	99.95 $^6H_{15/2}$ + 0.03 $^6F_{11/2}$ + 0.01 $^6H_{13/2}$
6	3505	Γ_8	3530.2	99.93 $^6H_{13/2}$ + 0.03 $^6H_{15/2}$ + 0.02 $^6H_{11/2}$
7		Γ_7	3532.1	99.88 $^6H_{13/2}$ + 0.08 $^6H_{15/2}$ + 0.02 $^6H_{11/2}$
8		Γ_7	3566.4	99.68 $^6H_{13/2}$ + 0.23 $^6H_{11/2}$ + 0.06 $^6F_{11/2}$
9		Γ_8	3576.4	99.79 $^6H_{13/2}$ + 0.12 $^6H_{11/2}$ + 0.04 $^6F_{11/2}$
10		Γ_6	3589.8	99.95 $^6H_{13/2}$ + 0.02 $^6H_{11/2}$ + 0.02 $^6H_{9/2}$
11	5833	Γ_6	5860.9	99.84 $^6H_{11/2}$ + 0.07 $^6F_{11/2}$ + 0.03 $^6H_{7/2}$
12		Γ_8	5867.6	99.72 $^6H_{11/2}$ + 0.09 $^6H_{9/2}$ + 0.08 $^6F_{9/2}$
13		Γ_7	5896.5	99.62 $^6H_{11/2}$ + 0.24 $^6H_{13/2}$ + 0.09 $^6F_{11/2}$
14		Γ_8	5909.0	99.77 $^6H_{11/2}$ + 0.09 $^6H_{13/2}$ + 0.06 $^6F_{11/2}$
15[e]		Γ_8	7707.9	78.72 $^6H_{9/2}$ + 21.04 $^6F_{11/2}$ + 0.13 $^6F_{9/2}$
16		Γ_8	7729.1	96.45 $^6H_{9/2}$ + 3.05 $^6F_{11/2}$ + 0.26 $^6F_{9/2}$
17		Γ_8	7749.0	98.56 $^6F_{11/2}$ + 1.31 $^6H_{9/2}$ + 0.05 $^6H_{11/2}$
18		Γ_6	7754.5	82.88 $^6H_{9/2}$ + 16.83 $^6F_{11/2}$ + 0.24 $^6F_{9/2}$
19		Γ_7	7758.4	99.83 $^6F_{11/2}$ + 0.09 $^6H_{11/2}$ + 0.07 $^6H_{13/2}$
20		Γ_6	7847.3	82.99 $^6F_{11/2}$ + 16.74 $^6H_{9/2}$ + 0.13 $^6H_{7/2}$
21		Γ_8	7851.6	77.12 $^6F_{11/2}$ + 22.69 $^6H_{9/2}$ + 0.12 $^6H_{11/2}$
22		Γ_8	9080.5	59.91 $^6F_{9/2}$ + 39.95 $^6H_{7/2}$ + 0.05 $^6H_{9/2}$
23		Γ_8	9149.8	99.34 $^6F_{9/2}$ + 0.40 $^6H_{7/2}$ + 0.11 $^6H_{9/2}$
24		Γ_7	9150.1	99.39 $^6H_{7/2}$ + 0.30 $^6H_{5/2}$ + 0.28 $^6F_{7/2}$
25		Γ_6	9162.2	88.08 $^6F_{9/2}$ + 11.55 $^6H_{7/2}$ + 0.30 $^6H_{9/2}$
26		Γ_6	9196.9	88.06 $^6H_{7/2}$ + 11.63 $^6F_{9/2}$ + 0.16 $^6F_{7/2}$
27		Γ_8	9214.4	59.02 $^6H_{7/2}$ + 40.10 $^6F_{9/2}$ + 0.43 $^6H_{5/2}$
28	10169	Γ_8	10200.2	99.22 $^6H_{5/2}$ + 0.35 $^6H_{7/2}$ + 0.15 $^6F_{7/2}$
29		Γ_7	10265.9	98.37 $^6H_{5/2}$ + 1.15 $^6F_{7/2}$ + 0.24 $^6H_{7/2}$
30	11025	Γ_7	11061.7	98.54 $^6F_{7/2}$ + 1.09 $^6H_{5/2}$ + 0.34 $^6H_{7/2}$
31		Γ_8	11089.9	99.78 $^6F_{7/2}$ + 0.16 $^6H_{5/2}$ + 0.03 $^6H_{9/2}$
32		Γ_6	11105.6	99.75 $^6F_{7/2}$ + 0.19 $^6H_{7/2}$ + 0.02 $^6H_{9/2}$

[a] $B_{40} = 710.4$ and $B_{60} = 48.97$ cm^{-1}.
[b] Numbers to designate levels used in discussion.
[c] Aqueous centroids.
[d] Irreducible representation of O group, Koster et al [8].
[e] Levels 15 through 27 are mixed. Centroids are $^6H_{9/2} = 7692$; $^6F_{11/2} = 7730$; $^6F_{9/2} = 9087$; and $^6H_{7/2} = 9115$ cm^{-1}.

of the $^6H_{15/2}$ to the $^6H_{13/2}$ were computed using equation (4) with $1 \le i \le 5$ and $6 \le j \le 10$ (table 8) and are shown in figure 5 for $T = 4.2$, 77, and 300 K. The g values for each state are given in table 9.

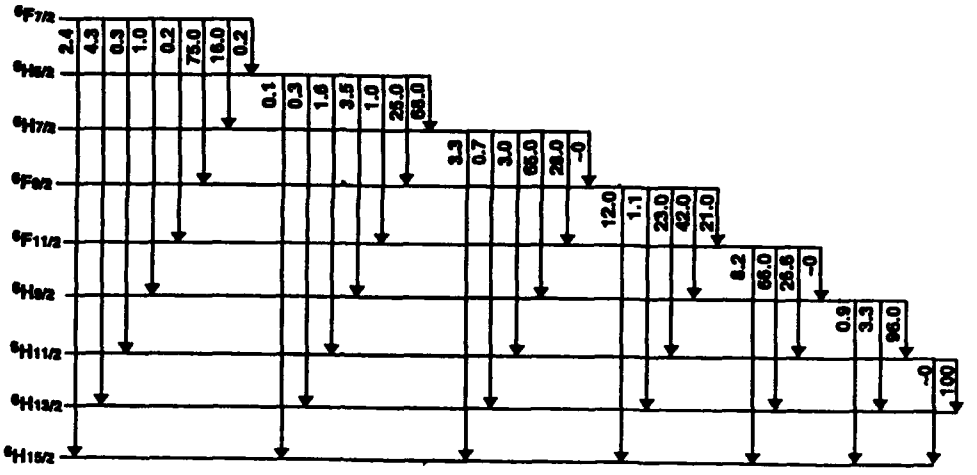

Figure 4. Multiplet-to-multiplet branching ratios for Dy^{3+} in DyAs.

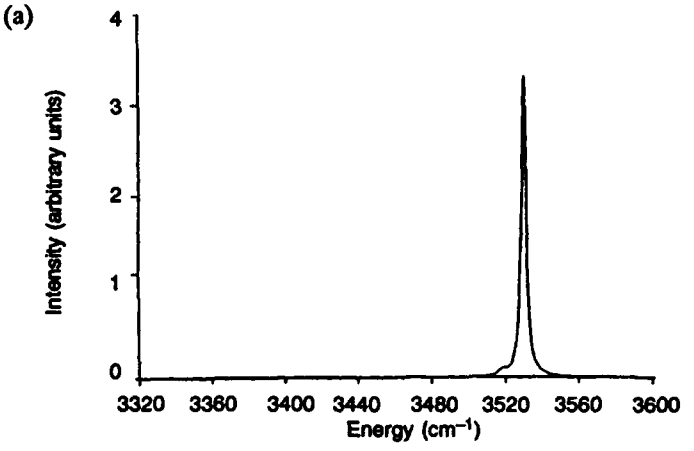

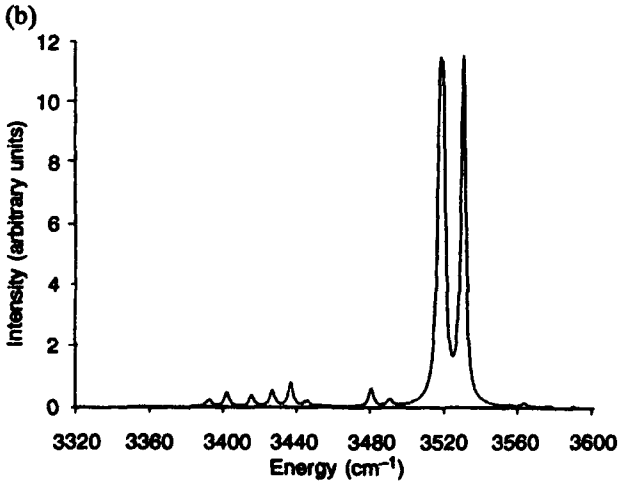

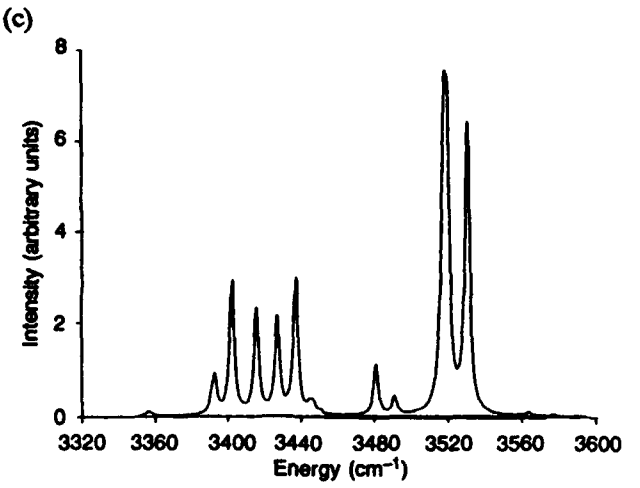

Figure 5. Predicted absorption spectra of $^6H_{15/2}$ to $^6H_{13/2}$ levels of Dy^{3+} in DyAs, assuming a Lorentzian line shape with $\Delta E = 3$ cm^{-1}: (a) $T = 4.2$ K, (b) $T = 77$ K, and (c) $T = 300$ K.

Table 9. Predicted g values for Γ_6, Γ_7, and Γ_8 levels of Dy^{3+} in DyAs[a]

No.	I. R.	g_1	g_2	No.	I. R.	g_1	g_2
1	Γ_6	-6.624	—	17	Γ_8	0.314	-10.742
2	Γ_8	-12.035	-0.908	18	Γ_6	2.415	—
3	Γ_7	—	7.514	19	Γ_7	—	-5.288
4	Γ_8	-5.335	10.394	20	Γ_6	-3.668	—
5	Γ_8	8.074	-11.703	21	Γ_8	8.544	2.668
6	Γ_8	0.525	11.245	22	Γ_8	-6.729	1.490
7	Γ_7	—	4.599	23	Γ_8	8.363	0.382
8	Γ_7	—	-3.723	24	Γ_7	—	2.303
9	Γ_8	-3.074	-6.908	25	Γ_6	4.330	—
10	Γ_6	6.339	—	26	Γ_6	-1.159	—
11	Γ_6	-4.387	—	27	Γ_8	-5.507	0.051
12	Γ_8	7.100	3.166	28	Γ_8	0.078	1.320
13	Γ_7	—	-4.442	29	Γ_7	—	-0.264
14	Γ_8	0.938	-9.698	30	Γ_7	—	4.124
15	Γ_8	5.879	2.836	31	Γ_8	-5.101	-1.358
16	Γ_8	-5.722	-0.403	32	Γ_6	-3.230	—

[a] *See Morrison et al [3] for definition of g values.*

7.3 Ho in HoAs

The energy levels and free-ion wavefunction composition for the ^5I_J multiplet of Ho^{3+} in HoAs for $J = 8$ to 5 are given in table 10. For each ^5I_J level, the composition of that state is practically 100 percent. The absorption spectra for the transitions between the energy levels of the $^5I_8$ to $^5I_7$ were computed using equation (4) with $1 \leq i \leq 7$ and $8 \leq j \leq 13$ (table 10) and are shown in figure 6 for $T = 4.2$, 77, and 300 K. The g values for each state are given in table 11.

Table 10. Predicted energy levels and free-ion mixture for Ho^{3+} in HoAs[a]

No.[b]	Centroid[c]	I. R.[d]	Energy (cm^{-1})	Free-ion mixture (%)
1	80	Γ_3	0.0	99.99 $^5I_8$
2		Γ_4	2.3	100.00 $^5I_8$
3		Γ_1	7.5	100.00 $^5I_8$
4		Γ_4	88.0	99.98 $^5I_8 + 0.01\ ^5I_7$
5		Γ_5	93.6	99.99 $^5I_8 + 0.01\ ^5I_7$
6		Γ_3	116.3	99.99 $^5I_8$
7		Γ_5	117.9	99.99 $^5I_8$
8	5116	Γ_4	5065.7	99.98 $^5I_7 + 0.01\ ^5I_8$
9		Γ_5	5068.9	99.99 $^5I_7 + 0.01\ ^5I_8$
10		Γ_2	5110.2	99.97 $^5I_7 + 0.02\ ^5I_6$
11		Γ_5	5120.6	99.97 $^5I_7 + 0.02\ ^5I_6$
12		Γ_3	5127.0	99.97 $^5I_7 + 0.02\ ^5I_6$
13		Γ_4	5139.7	99.99 $^5I_7 + 0.01\ ^5F_5$
14	8614	Γ_3	8570.7	99.97 $^5I_6 + 0.02\ ^5I_7$
15		Γ_5	8574.6	99.96 $^5I_6 + 0.02\ ^5I_7 + 0.01\ ^5I_5$
16		Γ_2	8590.8	99.97 $^5I_6 + 0.02\ ^5I_7$
17		Γ_5	8615.4	99.92 $^5I_6 + 0.07\ ^5I_5$
18		Γ_4	8625.7	99.94 $^5I_6 + 0.04\ ^5I_5$
19		Γ_1	8634.6	99.98 $^5I_6 + 0.01\ ^5I_4 + 0.01\ ^5F_4$
20	11164	Γ_4	11127.2	99.94 $^5I_5 + 0.04\ ^5I_6$
21		Γ_5	11144.8	99.92 $^5I_5 + 0.07\ ^5I_6$
22		Γ_3	11166.5	99.88 $^5I_5 + 0.11\ ^5I_4 + 0.01\ ^5F_4$
23		Γ_4	11174.1	99.9 $^5I_5 + 0.07\ ^5I_4 + 0.01\ ^5I_6$

[a] *$B_{40} = 705.4$ and $B_{60} = 51.11\ cm^{-1}$.*
[b] *Numbers to designate levels used in discussion.*
[c] *Aqueous centroids.*
[d] *Irreducible representation of O group, Koster et al [8].*

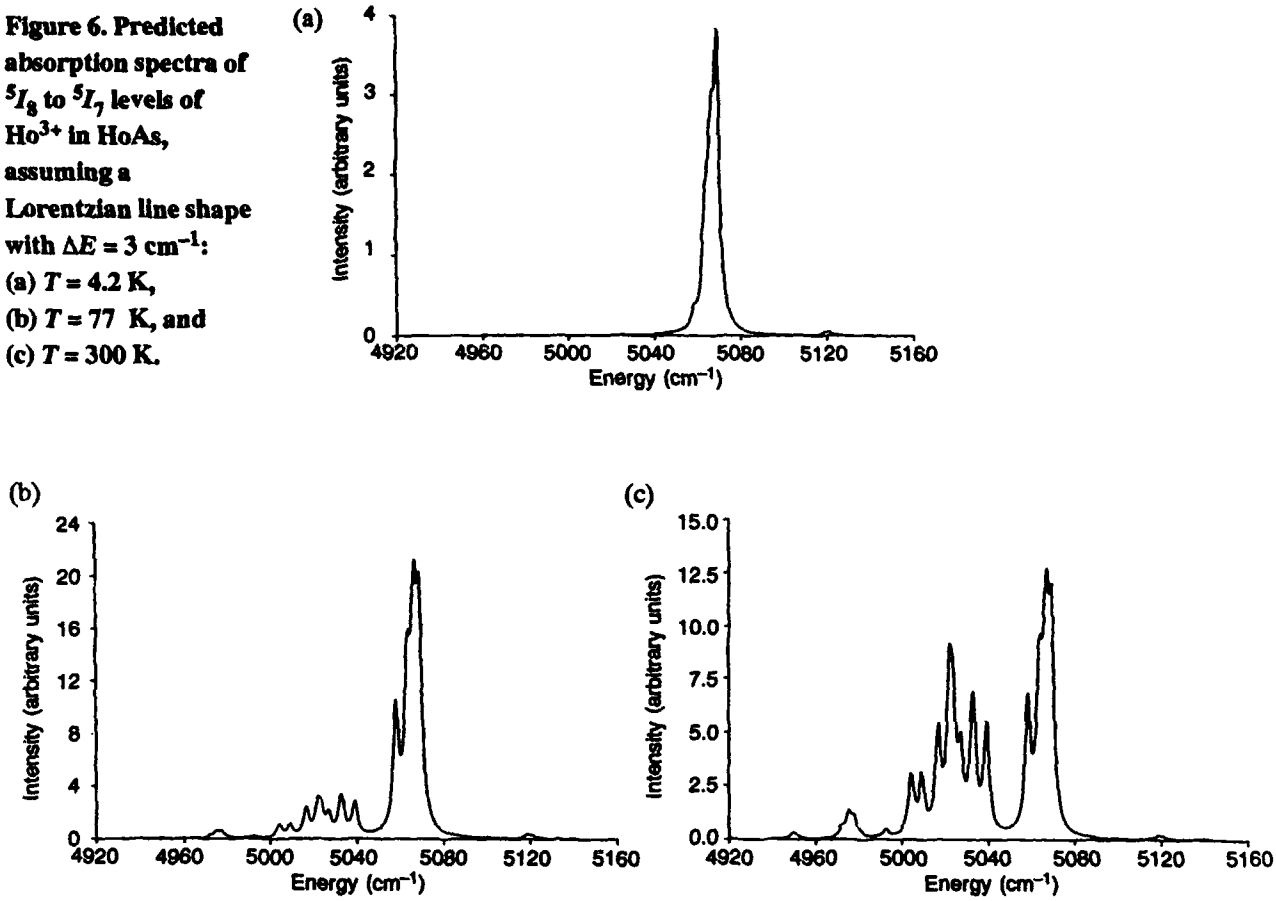

Figure 6. Predicted absorption spectra of $^5I_8$ to $^5I_7$ levels of Ho^{3+} in HoAs, assuming a Lorentzian line shape with $\Delta E = 3$ cm^{-1}: (a) $T = 4.2$ K, (b) $T = 77$ K, and (c) $T = 300$ K.

Table 11. Predicted g values for Γ_4 and Γ_5 levels of Ho^{3+} in HoAs[a]

No.	I. R.	g
2	Γ_4	–0.4529
4	Γ_4	–8.245
5	Γ_5	–9.6228
7	Γ_5	8.3998
8	Γ_4	–8.2079
9	Γ_5	–7.4662
11	Γ_5	–3.1396
13	Γ_4	9.3763
15	Γ_5	2.0476
17	Γ_5	3.2855
18	Γ_4	1.0616
20	Γ_4	5.4363
21	Γ_5	4.6125
23	Γ_4	–4.4706

[a] *See Morrison et al [3] for definitions of g values.*

7.4 Tm in TmAs

The energy levels and free-ion wavefunction composition for the $^3H_6$, $^3F_4$, and $^3H_5$ multiplet of Tm^{3+} in TmAs are given in table 12. Each of the $3H_J$ and $^3F_4$ consist of 100 percent of the free-ion level. These results indicate that the method of Lea et al [7] would be applicable to all the multiplets. The absorption spectra for the transitions between the energy levels of $^3H_6$ to the $^3F_4$ were computed using equation (4) with $1 \le i \le 6$ and $7 \le j \le 10$ (table 12) and are shown in figure 7 for $T = 4.2$, 77, and 300 K. The g values for all the levels are given in table 13.

In 1979, Hulliger [10] listed four different sets of experimental energy levels for the $^3H_6$ multiplet as given in table 14. Table 15 compares our results with Hulliger's. In almost all cases, our predicted values lie within the variance of the experimental energy levels given in table 14.

Table 12. Predicted energy levels and free-ion mixture for Tm^{3+} in TmAs[a]

No.[b]	Centroid[c]	I. R.[d]	Energy (cm^{-1})	Free-ion mixture (%)	
1	202	Γ_1	0.0	99.91	$^3H_6 + 0.08\ ^3F_4$
2		Γ_4	28.7	99.95	$^3H_6 + 0.04\ ^3F_4$
3		Γ_5	62.9	99.98	$^3H_6 + 0.01\ ^3F_4 + 0.01\ ^3H_5$
4		Γ_2	145.7	100.00	$^3H_6$
5		Γ_5	201.9	99.99	$^3H_6$
6		Γ_3	215.5	99.98	$^3H_6 + 0.01\ ^3F_4$
7	5812	Γ_5	5620.6	99.98	$^3F_4 + 0.01\ ^3H_6 + 0.01\ ^3H_4$
8		Γ_3	5750.3	99.91	$^3F_4 + 0.07\ ^3H_5 + 0.01\ ^3H_6$
9		Γ_4	5778.2	99.91	$^3F_4 + 0.05\ ^3H_5 + 0.04\ ^3H_6$
10		Γ_1	5815.6	99.91	$^3F_4 + 0.08\ ^3H_6$
11	8390	Γ_9	8225.6	99.90	$^3H_5 + 0.05\ ^3F_4 + 0.03\ ^3H_4$
12		Γ_3	8244.8	99.83	$^3H_5 + 0.08\ ^3H_4 + 0.07\ ^3F_4$
13		Γ_5	8331.5	99.96	$^3H_5 + 0.01\ ^3F_2 + 0.01\ ^3H_6$
14		Γ_4	8380.2	99.97	$^3H_5 + 0.02\ ^3H_4$
15	12720	Γ_5	12569.9	99.63	$^3H_4 + 0.33\ ^3F_3 + 0.04\ ^3F_2$
16		Γ_3	12622.4	99.81	$^3H_4 + 0.11\ ^3F_2 + 0.08\ ^3H_5$
17		Γ_4	12664.3	99.85	$^3H_4 + 0.10\ ^3F_3 + 0.05\ ^3H_5$
18		Γ_1	12724.4	99.99	$^3H_4$

[a] $B_{40} = 705.1$ and $B_{60} = 51.48\ cm^{-1}$.
[b] Numbers to designate levels used in discussion.
[c] Aqueous centroids.
[d] Irreducible representation of O group, Koster et al [8].

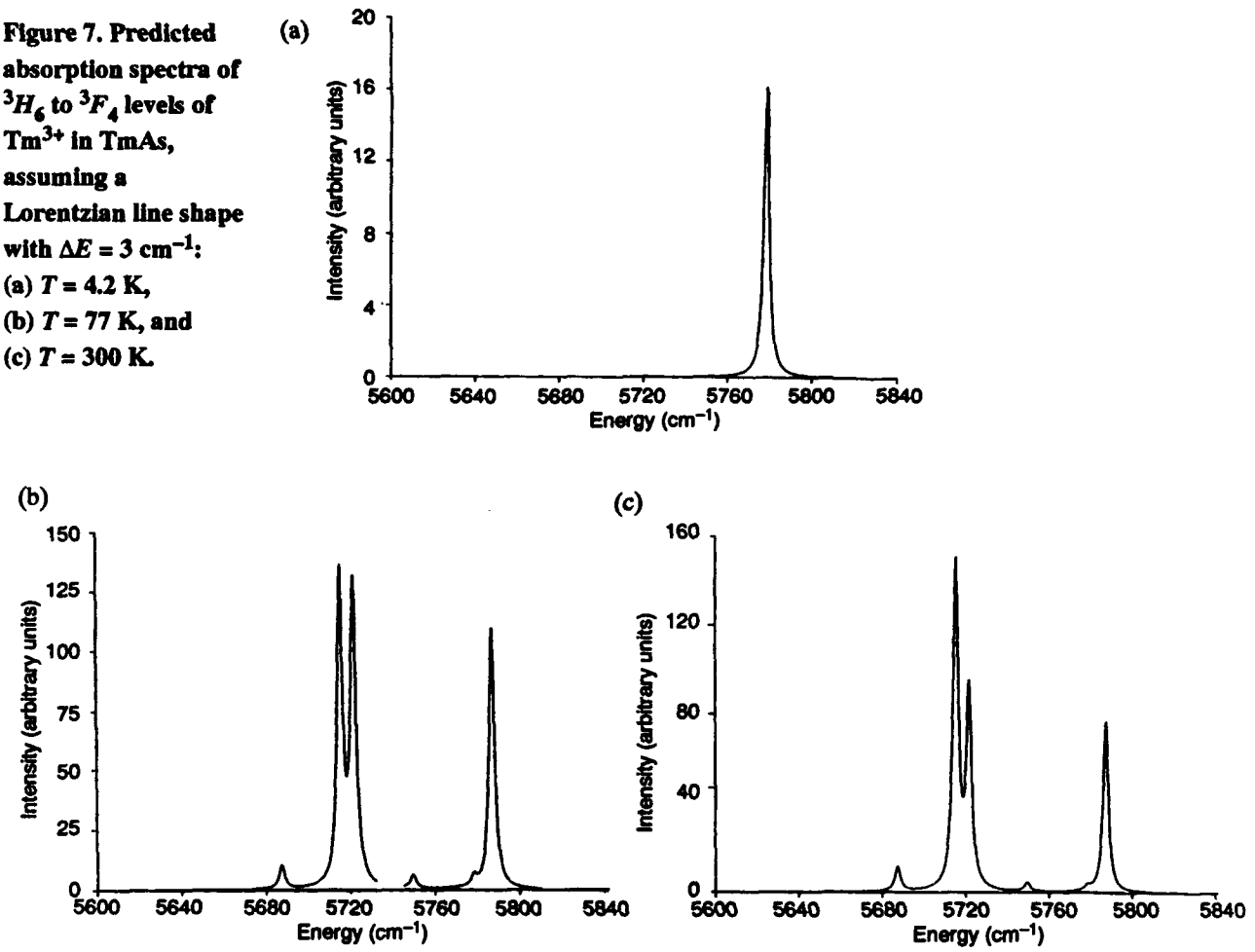

Figure 7. Predicted absorption spectra of $^3H_6$ to $^3F_4$ levels of Tm^{3+} in TmAs, assuming a Lorentzian line shape with $\Delta E = 3$ cm^{-1}: (a) $T = 4.2$ K, (b) $T = 77$ K, and (c) $T = 300$ K.

Table 13. Predicted g values for Γ_4 and Γ_5 levels of Tm^{3+} in TmAs[a]

No.	I. R.	g
2	Γ_4	1.1755
3	Γ_5	3.5743
5	Γ_5	2.2514
7	Γ_5	–5.6900
9	Γ_4	1.1394
11	Γ_4	–5.0612
13	Γ_5	5.1658
14	Γ_4	6.0613

[a]See Morrison et al [3] for definitions of g values.

Table 14. Experimental energy levels (cm^{-1}) of Tm^{3+} in TmAs reported by Hulliger [10][a]

No.[b]	I. R.	1	2	3	4
2	Γ_4	21.5	21.5	19.5	23.6
3	Γ_5	46.5	48.7	41.7	50.7
4	Γ_2	139	101	124	152
5	Γ_5	165	162	148	181
6	Γ_3	174	174	156	190

[a]See Hulliger [10] for references to experimental data. Hulliger's data are multiplied by 0.6950 cm^{-1}/K.

[b]Numbers correspond to table 12: ground state is Γ_1.

Table 15. Comparison of present work and Hulliger [10]

Level	Energy levels (cm^{-1})	
	Present work	1979, Hulliger
2 (Γ_4)	28.7	19.5–23.6
3 (Γ_5)	62.9	41.7–50.7
4 (Γ_2)	145.7	101–152
5 (Γ_5)	201.9	148–181
6 (Γ_3)	215.5	156–190

7.5 Yb in YbAs

The energy levels and free-ion wavefunction composition for the two multiplets, $^2F_{7/2}$ and $^2F_{5/2}$, of Yb^{3+} in YbAs are given in table 16. The J mixing by the crystal field is negligible, and each level is practically 100 percent of that multiplet (99.99 percent). The absorption spectra for the transitions between the energy levels of the $^2F_{7/2}$ to the $^2F_{5/2}$ were computed using equation (4) with $1 \leq i \leq 3$ and $4 \leq j \leq 5$ (table 16) and are shown in figure 8 for $T = 4.2$, 77, and 300 K. The g values for each level are given in table 17. The energy levels of the $^4F_{7/2}$ have recently been determined by inelastic neutron scattering in 1990 by Kohgi et al [11]. They report the first excited state, Γ_8, at 144 cm^{-1} at $T = 14$ K, and at 200 K they report the Γ_8 at 152 cm^{-1} and the Γ_7 at 340 cm^{-1}. In 1991, Donni et al [12] reported the Γ_8 at 141 cm^{-1} and the Γ_7 at 331 cm^{-1}; these measurements were made over a temperature range of 40 to 295 K. Both Kohgi et al [11] and Donni et al [12] found their experimental data consistent with a Γ_6 ground level. We calculated the line strength for the $\Gamma_6 \rightarrow \Gamma_8$ to be 558×10^{-23} cm^2 and the $\Gamma_8 \rightarrow \Gamma_8$ line strength to be 358×10^{-23} cm^2, which qualitatively agrees with the plots of Donni et al [12].

Table 16. Predicted energy levels and free-ion mixture for Yb^{3+} in YbAs[a]

No.[b]	Centroid[c]	I. R.[d]	Energy (cm^{-1})	Free-ion mixture (%)
1	250	Γ_6	0.0	100.00 $^2F_{7/2}$
2		Γ_8	128.6	99.99 $^2F_{7/2}$ + 0.01 $^2F_{5/2}$
3		Γ_7	293.7	99.99 $^2F_{7/2}$ + 0.01 $^2F_{5/2}$
4	10450	Γ_8	10272.9	99.99 $^2F_{5/2}$ + 0.01 $^2F_{7/2}$
5		Γ_7	10471.8	99.99 $^2F_{5/2}$ + 0.01 $^2F_{7/2}$

[a] *$B_{40} = 697.0$ and $B_{60} = 49.85$ cm^{-1}.*
[b] *Numbers to designate levels used in discussion.*
[c] *Aqueous centroids.*
[d] *Irreducible representation of O group, Koster et al [8].*

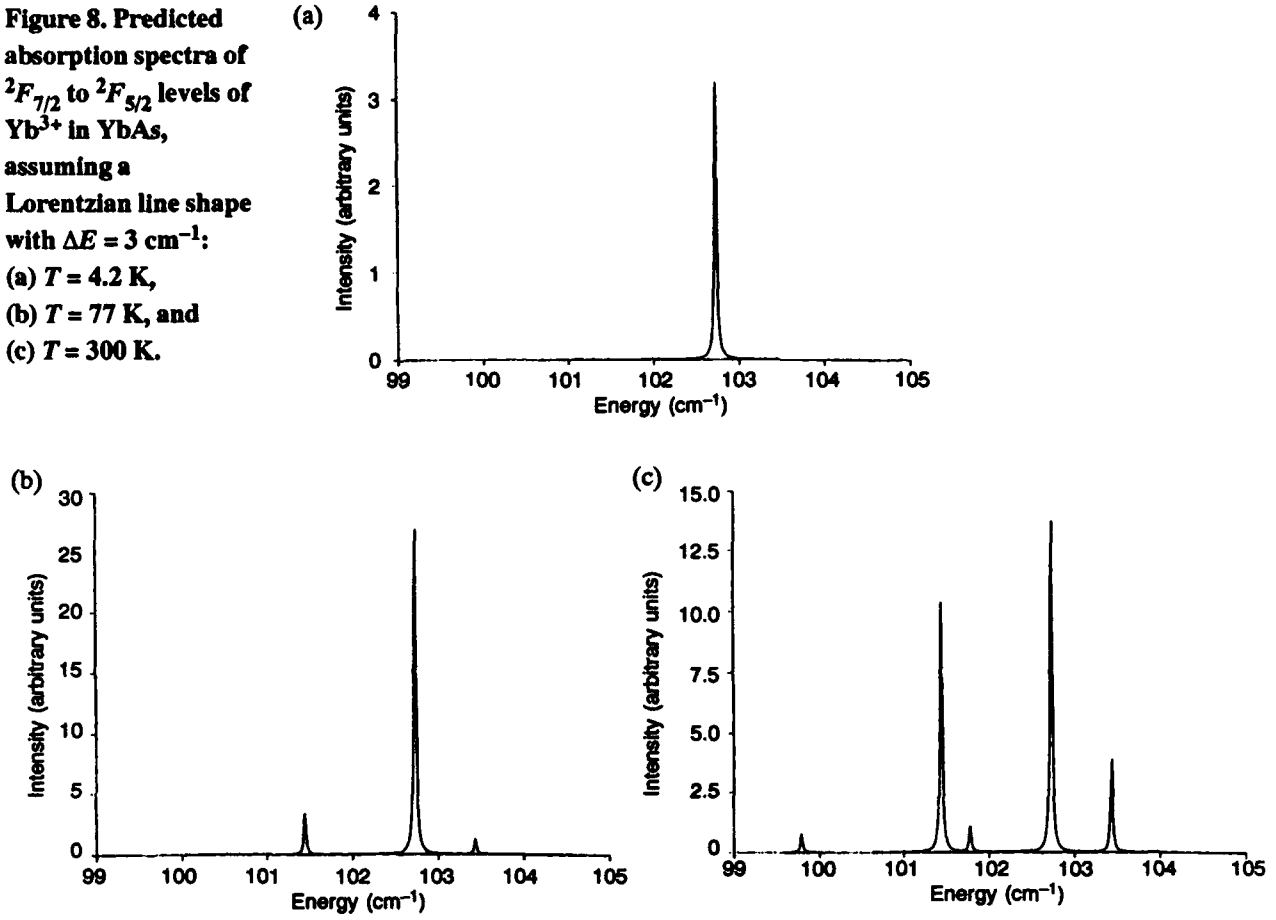

Figure 8. Predicted absorption spectra of $^2F_{7/2}$ to $^2F_{5/2}$ levels of Yb^{3+} in YbAs, assuming a Lorentzian line shape with $\Delta E = 3$ cm^{-1}:
(a) $T = 4.2$ K,
(b) $T = 77$ K, and
(c) $T = 300$ K.

Table 17. Predicted g values for Γ_6, Γ_7, and Γ_8 of Yb^{3+} in YbAs[a]

No.	I. R.	g_1	g_2
1	Γ_6	–2.667	—
2	Γ_8	–4.179	–1.155
3	Γ_7	—	3.419
4	Γ_8	0.8442	3.153
5	Γ_7	—	–1.417

[a]See Morrison et al [3] for definitions of g values.

8. Conclusion

We have used a crystal-field Hamiltonian appropriate for a rare-earth ion in octahedral cubic symmetry and varied two crystal-field parameters, B_{40} and B_{60}, to obtain the best fit to the experimental data of Schneider et al [2] taken on Er^{3+} in ErAs. We also calculated the optical absorption data and obtained excellent agreement with the results of their traces taken at 5, 74, and 300 K.

Using scaling and interpolation procedures, we obtained phenomenological A_{nm} for the entire *Ln*As series (*Ln* = La to Lu). No attempt at a more fundamental theory of the A_{nm} (such as given in 1991 by Stevens and Morrison [13]) was considered. The phenomenological A_{nm} then yielded B_{nm} for the *Ln*As series from which energy levels below the band gap of GaAs, g values, and multiplet branching ratios were calculated for the rare-earth ions Tb^{3+} through Yb^{3+}. The energy levels of the ground multiplet of Tm^{3+} and Yb^{3+} in their respective arsenide compounds are in reasonable agreement with the energy levels determined by inelastic neutron scattering experiments. Calculated absorption spectra at 4.2 to 300 K are also given for the lowest lying multiplets for Tb^{3+} through Yb^{3+} in their respective arsenide compounds. The g values for all the levels in all the compounds are calculated.

Acknowledgements

Greg Turner, Wayne Lee, and Baruch Sheinson are thanked for their help with the calculations and graphing.

References

1. W. T. Tsang and R. A. Logan, Appl. Phys. Lett. **49** (1986), 1686.

2. J. Schneider, H. D. Müller, J. D. Ralston, F. Fuchs, A. Dörnen, and K. Thonke, *Crystal-Field Splittings of Er^{3+} ($4f^{11}$) in Molecular Beam Epitaxially Grown ErAs/GaAs,* Appl. Phys. Lett. **59** (1991), 34.

3. C. A. Morrison, D. E. Wortman, and R. P. Leavitt, J. Chem. Phys. **73** (1980), 2580. (This paper should be consulted for a complete detailed description of the methods used in the analysis presented here.)

4. C. A. Morrison and R. P. Leavitt, J. Chem. Phys. **71** (1979), 2366.

5. R.W.G. Wyckoff, *Crystal Structures,* vol.1 (1968), 85–91.

6. W. T. Carnall, P. R. Fields, and K. Rajnak, J. Chem. Phys. **49** (1968), 4412, 4424, 4443, 4447, and 4450 (five consecutive papers).

7. K. R. Lea, M.J.M. Leask, and W. P. Wolf, J. Phys. Chem. Solids **23** (1962), 1381.

8. G. F. Koster, J. O. Dimmock, R. G. Wheeler, and H. Statz, *Properties of the Thirty-Two Point Groups,* MIT Press, Cambridge, Massachusetts (1963).

9. R. P. Leavitt, C. A. Morrison, and D. E. Wortman, *Rare Earth Ion-Host Crystal Interactions 3. Three Parameter Theory of Crystal Fields,* Harry Diamond Laboratories, HDL-TR-1673 (June 1975).

10. F. Hulliger, *Rare Earth Pnictides,* in *Handbook on the Physics and Chemistry of Rare Earths,* ed. K. A. Gschneidner, Jr., and L. Eyring, vol. 4 (1979), 153.

11. M. Kohgi, K. Ohoyama, A. Oyamada, T. Suzuki, and M. Arai, Physica **B163** (1990), 625.

12. A. Donni, A. Furrer, P. Fischer, F. Hulliger, and P. Wachter, Physica **B171** (1991), 353.

13. Sally B. Stevens and Clyde A. Morrison, *Theoretical Crystal-Field Calculations for Rare-Earth Ions in III-V Semiconductor Compounds,* Harry Diamond Laboratories, HDL-TM-91-16 (October 1991).

Distribution

Administrator
Defense Technical Information Center
Attn: DTIC-DDA (2 copies)
Cameron Station, Building 5
Alexandria, VA 22304-6145

Director
Defense Advanced Research Projects Agency
Attn: A. Yang
1400 Wilson Blvd
Arlington, VA 22290

Defense Nuclear Agency
Attn: TITL, Tech Library
6801 Telegraph Road
Alexandria, VA 22310-3398

Under Secretary of Defense Research & Engineering
Attn: Technical Library, 3C128
Washington, DC 20301

Commander
Atmospheric Sciences Laboratory
Attn: Technical Library
White Sands Missile Range, NM 88002

Director
Night Vision & Electro-Optics Lab, LABCOM
Attn: A. Pinto (2 copies)
Attn: J. Daunt
Attn: L. Merkel
Attn: R. Buser
Attn: Technical Library
Attn: W. Tressel
Attn: B. Zandi
FT Belvoir, VA 22060

Office of the Deputy Chief of Staff for Res, Devl, & Acq
Attn: DAMA-ARZ-B, I. R. Hershner
Department of the Army
Washington, DC 20310

Director
US Army Ballistics Research Laboratory
Attn: SLCBR-DD-T (STINFO)
Aberdeen Proving Ground, MD 21005

Director
US Army Electronics Warfare Laboratory
Attn: C. Thornton
Attn: T. Aucoin
Attn: AMSEL-DD, M. Thompsett
FT Monmouth, NJ 07703

Commander
US Army Materials & Mechanics Research Center
Attn: SLCMT-TL, Tech Library
Watertown, MA 02172

Commander
US Army Missile & Munitions Center & School
Attn: AMSMI-TB, Redstone Sci Info Center
Attn: ATSK-CTD-F
Redstone Arsenal, AL 35809

Commander
US Army Research Office Durham
Attn: J. Mink
Attn: G. Iafrate
Attn: M. Ciftan
Attn: M. Strosio
Attn: R. Guenther
PO Box 12211
Research Triangle Park, NJ 27709

Commander
US Army Test & Evaluation Command
Attn: D. H. Sliney
Attn: Tech Library
Aberdeen Proving Ground, MD 21005

Distribution (cont'd)

Commander
US Army Troop Support Command
Attn: STRNC-RTL, Tech Library
Natick, MA 01762

Commanding Officer
US Foreign Science & Technology Center
Attn: AIAST-BS, Basic Science Div
Federal Office Building
Charlottesville, VA 22901

Director
Naval Research Laboratory
Attn: A. Rosenbaum
Attn: Code 2620, Tech Library Br
Attn: Code 5554, F. Bartoli
Attn: Code 5554, L. Esterowitz
Attn: Code 5554, R. E. Allen
Attn: G. Risenblatt
Washington, DC 20375

Commander
Naval Weapons Center
Attn: Code 3854, M. Hills
Attn: Code 3854, M. Nader
Attn: Code 3854, R. L. Atkins
Attn: Code 3854, R. Schwartz
Attn: DOCE343, Technical Information Dept
China Lake, CA 93555

National Institute of Standards & Technology
Attn: Library
Gaithersburg, MD 20899

Ames Laboratory Dow Iowa State University
Attn: K. A. Gschneidner, Jr. (2 copies)
Ames, IA 50011

Argonne National Laboratory
Attn: W. T. Carnall
9700 South Cass Avenue
Argonne, IL 60439

Oak Ridge National Laboratory
Attn: R. G. Haire
Oak Ridge, TN 37839

Allied Signal Inc
Attn: R. Morris
POB 1021 R
Morristown, NJ 07960

NASA Langley Research Center
Attn: C. Bair
Attn: E. Filer
Attn: G. Armagen
Attn: J. Barnes
Attn: M. Buoncristiani
Attn: N. P. Barnes (2 copies)
Attn: P. Cross
Attn: D. Getteny
Hampton, VA 23665

National Oceanic & Atmospheric
Adm Environmental Research Labs
Attn: Library, R-51, Tech Rpts
Boulder, CO 80302

Arizona State University Dept of Chemistry
Attn: L. Eyring
Tempe, AZ 85281

Colorado State University
Physics Department
Attn: S. Kern
FT Collins, CO 80523

Departmento De Química Fundamental and
Departmento de Fisica
Attn: A. da Gama
Attn: G. F. de Sá
Attn: O. L. Malta
da UFPE, Cidade Universitaria
50,000, Recife, Pe, Brasil

Distribution (cont'd)

Howard University Department of Physics
Attn: Prof. V. Kushamaha
25 Bryant St., NW
Washington, DC 20059

Johns Hopkins University Dept of Physics
Attn: B. R. Judd
Baltimore, MD 21218

Kalamazoo College Dept of Physics
Attn: K. Rajnak
Kalamazoo, MI 49007

Massachusetts Institute of Technology
Crystal Physics Laboratory
Attn: H. P. Jenssen
Cambridge, MA 02139

Pennsylvania State University
Materials Research Laboratory
Attn: W. B. White
University Park, PA 16802

Princeton University
Department of Chemistry
Attn: D. S. McClure
Attn: C. Weaver
Princeton, NJ 08544

San Jose State University
Department of Physics
Attn: J. B. Gruber
San Jose, CA 95192

Seton Hall University
Chemistry Department
Attn: H. Brittain
South Orange, NJ 07099

U.P.R 210 C.N.R.S
Attn: M. Faucher
Attn: P. Caro
Attn: P. Porcher
1 Place A-Briand, 92195 Meudon Cédex,
France

University of Connecticut
Department of Physics
Attn: R. H. Bartram
Storrs, CT 06269

University of Dayton
Department of Chemistry
Attn: S. P. Sinha
300 College Park
Dayton, OH 45469-2350

University of Illinois Everitt Lab
Attn: J. G. Eden
1406 W. Green St
Urbana, IL 61801

University of Illinois
Gaseous Electronics Laboratory
Attn: S. B. Stevens
607 E. Healey St
Champaign, IL 61820

University of Michigan
Dept of Physics
Attn: S. C. Rand
Ann Arbor, MI 48109

University of Minnesota, Duluth
Department of Chemistry
Attn: L. C. Thompson
Duluth, MN 55812

University of South Florida
Physics Department
Attn: R. Chang
Attn: Sengupta
Tampa, FL 33620

University of Southern California
Attn: M. Birnbaum
Los Angeles, CA 90089

University of Virginia Dept of Chemistry
Attn: F. S. Richardson (2 copies)
Attn: J. Quagliano
Charlottesville, VA 22901

Distribution (cont'd)

University of Wisconsin
Chemistry Department
Attn: B. Tissue
Attn: J. Wright
Madison, WI 53706

Aerospace Corporation
Attn: N. C. Chang
PO Box 92957
Los Angeles, CA 90009

Department of Mech, Indus,
& Aerospace Eng
Attn: S. Temkin
PO Box 909
Piscataway, NJ 08854

Engineering Societies Library
Attn: Acquisitions Department
345 East 47th St.
New York, NY 10017

Fibertech, Inc.
Attn: H. R. Verdin (3 copies)
510-A Herdon Pkwy
Herdon, VA 22070

Hughes Aircraft Company
Attn: D. Sumida
3011 Malibu Canyon Rd
Malibu, CA 90265

IBM Research Division
Almaden Research Center
Attn: R. M. Macfarlane,
Mail Stop K32 802(d)
650 Harry Road
San Jose, CA 95120

Institute for Low Temp & Struc Rsch
Polish Academy of Sciences
Attn: R. Troc
50-950 Wroclaw, PO Box 937,
ul. Okólna 2, Poland

Lawrence Berkeley Laboratory
Attn: N. Edelstein, MS70A-1150
Berkeley, CA 94720

Director
Lawrence Radiation Laboratory
Attn: H. A. Koehler
Attn: M. J. Weber
Attn: W. Krupke
Livermore, CA 94550

Lightning Optical Corp
Attn: G. Quarles
431 East Spruce St.
Tarpon Springs, FL 34689

LTV
Attn: M. Kock (WT-50)
PO Box 650003
Dallas, GX 75265

Martin Marietta
Attn: P. Caldwell
Attn: F. Crowne
Attn: J. Little
Attn: T. Worchesky
1450 South Rolling Rd
Baltimore, MD 21227

McDonnell Douglass Electronic Systems
Company
Attn: Dept Y440 Bldg. 101, Lev. 2Rm/PTB54,
D. M. Andrauskas, MS-2066267
PO Box 516
ST Louis, MO 63166

MIT Lincoln Lab
Attn: B. Aull
PO Box 73
Lexington, MA 02173

Montana Analytic Services
Attn: M. Schwan
325 Icepond Rd
Bozeman, MT 59715

Distribution (cont'd)

Science Applications International Corp
Attn: T. Allik
1710 Goodridge Drive
McLean, VA 22102

Southwest Research Institute
Attn: M. J. Sablik
PO Brawer 28510
San Antonio, TX 78228-0510

Swartz Electro-Optic, Inc
Attn: G. A. Rines
45 Winthrop Street
Concord, MA 01742

Union Carbide Corp
Attn: M. R. Kokta
50 South 32nd Street
Washougal, WA 98671

W. J. Schafer Assoc
Attn: J. W. Collins
321 Ballerica Road
Chelmsford, MA 01824

US Army Laboratory Command
Attn: AMSLC-DL, Dir Corp Labs

Installation Support Activity
Attn: SLCIS-CC-IP, Legal Office

USAISC
Attn: AMSLC-IM-VA, Admin Ser Br
Attn: AMSLC-IM-VP, Tech Pub Br
(2 copies)

Harry Diamond Laboratories
Attn: Laboratory Directors
Attn: SLCHD-CS, Chief Scientist
Attn: SLCHD-NW-EH, Chief
Attn: SLCHD-NW-EP, C. S. Kenyon
Attn: SLCHD-NW-EP, Chief
Attn: SLCHD-NW-EP, J. R. Miletta
Attn: SLCHD-NW-ES, Chief
Attn: SLCHD-NW-P, Chief
Attn: SLCHD-NW-RF, Chief
Attn: SLCHD-NW-RP, B. McLean
Attn: SLCHD-NW-RP, Chief
Attn: SLCHD-NW-RS, L. Libelo
Attn: SLCHD-NW-TN, Chief
Attn: SLCHD-NW-TS, Chief
Attn: SLCHD-PO, Chief
Attn: SLCHD-SD-TL, Library (3 copies)
Attn: SLCHD-SD-TL, Library (Woodbridge)
Attn: SLCHD-ST-AP, C. Morrison (10 copies)
Attn: SLCHD-ST-AP, D.Wortman
(10 copies)
Attn: SLCHD-ST-AP, E. Harris
Attn: SLCHD-ST-AP, G. Simonis
Attn: SLCHD-ST-AP, J. Bradshaw
Attn: SLCHD-ST-AP, J. Bruno
Attn: SLCHD-ST-AP, J. Pham
Attn: SLCHD-ST-AP, M. Stead
Attn: SLCHD-ST-AP, M. Tobin
Attn: SLCHD-ST-AP, R. Leavitt
Attn: SLCHD-ST-AP, R. Tober
Attn: SLCHD-ST-AP, T. Bahder
Attn: SLCHD-ST-OP, C. Garvin
Attn: SLCHD-ST-OP, J. Goff
Attn: SLCHD-ST-R, A. A. Bencivenga
Attn: SLCHD-ST-SP, Chief
Attn: SLCHD-ST-SP, J. Nemarich
Attn: SLCHD-ST-SS, Chief
Attn: SLCHD-TA-AS, G. Turner
Attn: SLCHD-TA-ET, B. Zabludowski